THE JOURNAL OF PHYSICAL CHEMISTRY A

pubs.acs.org/JPCA

Article

Rate-Limiting Steps in the Intramolecular C−H Activation of Ruthenium N-Heterocyclic Carbene Complexes

Katarzyna Młodzikowska-Pieńko* and Bartosz Trzaskowski*

Cite This: *J. Phys. Chem. A* 2020, 124, 3609−3617

Read Online

ACCESS | Metrics & More | Article Recommendations | Supporting Information

ABSTRACT: Ruthenium (II) complexes with N-heterocyclic carbenes (NHC) are commonly used as efficient catalysts in hydrogenation of olefins with simultaneous intramolecular C−H activation. Using the DFT approach, we have investigated the entire hydrogenation reaction pathway for four new potential catalysts and ethylene, a model substrate. Our calculations imply that the dissociation of phosphine is the rate-limiting step of hydrogenation, contrary to recent computational results. We also found that catalysts bearing NHCs with aliphatic and aromatic side groups are energetically favorable over other aliphatic cyclohexyl-substituted NHC. To examine how electronic properties of various catalysts influence the energetic barrier in the crucial steps of the reaction, we applied the Noncovalent Interaction analysis, which allowed us to reveal crucial interactions which stabilize/destabilize important intermediates and transition states in the hydrogenation reaction.

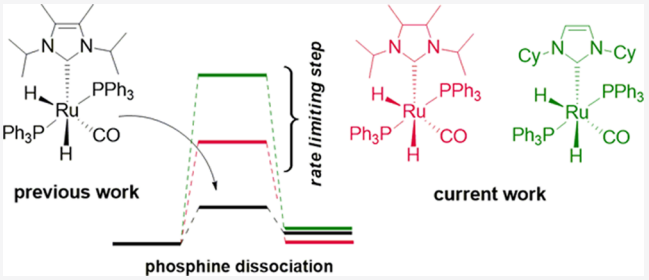

INTRODUCTION

Even though less than 30 years has passed since the synthesis of the first stable carbene by Arduengo, it is difficult to imagine today's catalysis without these versatile ligands.[1] Used extensively both in organocatalysis and transition-metal catalysis, they have become one of the most commonly used ligands for many catalytic processes.[2−6] Historically, the first group of carbenes were N-heterocyclic carbenes (NHCs) and they found numerous uses in a large number of catalytic processes, with the most successful story being the olefin metathesis catalyzed by NHC-ruthenium complexes.[7,8] During this catalytic reaction, the olefin is associated to the ruthenium core of the catalyst and then undergoes a series of transformations leading to the interchange of its substituents. This process can also occur through the association mechanism, where the activation of the catalyst is preceded by association of the substrate.[9,10] The relatively strong interaction between the ruthenium and the olefin may, however, be also used in other chemical transformations, such as, for example, hydrogenation.[11] Unlike transfer hydrogenation of ketones, for which there are many known and efficient ruthenium catalysts,[12,13] the number of Ru catalyst containing a Ru−H bond for direct hydrogenation of alkenes is relatively low. The first example of such system, synthesized in 2001 by the Nolan group, is an active catalyst in hydrogenation of alkenes with TONs up to 24,000 h^{-1}.[14] Since then, other but structurally similar complexes bearing either one or two NHCs have been synthesized and used in hydrogenation (see Figure 1).[15−19]

One of the most interesting features of this type of complexes is the fact that upon hydrogenation, a reactive Ru center may also force C−H bond activation. Catalytic functionalization of the unreactive C−H bond is one of the most important recent developments in synthetic methodologies allowing for faster and more efficient production of various groups of chemical compounds.[20,21] Today, there is a large number of transition-metal complexes, including Pd, Pt, Fe, Rh, Ir and others that facilitate C−H bond activation.[22−26] Ruthenium has been also commonly used in C−H bond activation, although as relatively simple complexes of either Ru(0) or Ru(II), such as $[RuCl_2(C_6H_6)]_2$ or $[RuCl_2(p\text{-cymene})]_2$.[27] The phenomenon of C−H activation is primarily characteristic for NHC ligands, during which the electronic properties and catalytic activity of the NHCs are altered.[28,29] The advantage of a catalyst performing subsequent hydrogenation and C−H activation is the possibility to use it in more complex tandem reactions. In the case of ruthenium complexes, the best known example of such activity is the tandem alcohol dehydrogenation/Wittig reaction/alkene hydrogenation reaction performed by the Williams catalyst.[30]

These catalysts have been also subject to a number of computational mechanistic studies. Whittlesey studied the C−H activation process of Williams catalyst using density functional theory (DFT) methods and base-induced mechanism.[31] The same group studied also H_2 loss and C−H activation in Edney

Received: February 17, 2020
Revised: April 14, 2020
Published: April 15, 2020

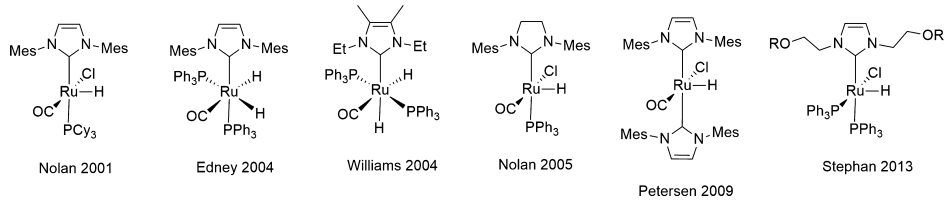

Figure 1. Ruthenium complexes bearing NHCs used in hydrogenation.

complexes[32] as well as performed comparative analysis of the influence of substituents in the aryl group on the activation of C(aryl)−X bond activation.[33] Finally, a very thorough mechanistic study of the entire catalytic cycle of the Williams catalyst and its hydride chloride derivative has been performed recently by Houk and co-workers.[34] In this work, he explored the mechanism of a tandem alkene hydrogenation/intramolecular C−H activation and showed that the Williams catalyst reacts via a dissociative process with stepwise hydride migration, reductive elimination, and oxidative addition via a Ru(0) intermediate, as originally suggested by Whittlesey. On the other hand, the hydride chloride complex is activated through a reactive Ru(IV) intermediate (Figure 2).

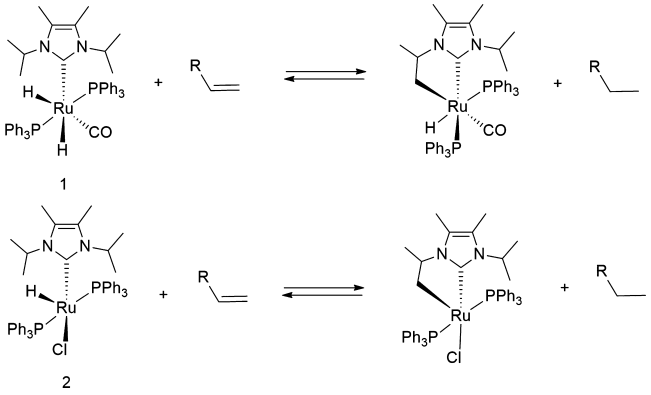

Figure 2. Alkene hydrogenation and coupled intramolecular C−H activation of complex (**1**) and alkene hydrogenation and coupled intramolecular C−H activation of complex (**2**).

Interestingly, there are virtually no studies on the structure−activity relationships for this class of complexes. This is even more surprising given the fact that there are hundreds of known NHCs and a large number of studies on how the structural changes in carbenes affect the catalytic activities of ruthenium olefin metathesis catalysts.[3,7,8,35−38] In this work, we show how small changes in NHC side groups affect the Gibbs free energy barriers for tandem hydrogenation/C−H activation of derivatives of **1** (Figure 3) as well as take a closer look at the rate-limiting steps for this type of reaction. To perform this task, we performed computational studies on the catalytic pathway for five different catalysts including **1** and four similar systems with structural changes in the carbene part, based on crystal structures of known NHCs, commonly used in various Ru catalysts (**3**−**5**, Figure 3).[16,30,39−42]

THEORETICAL METHODS

In our work, we have used the DFT approach similar to our previous studies[35,37,38,43] to investigate the ethylene hydrogenation and ruthenacyclization pathways for four catalysts: **3**, **4**, **5**, and **6** (Figure 3). All stationary points were fully optimized at the B3LYP/LACVP** level of theory in vacuum. For more accurate values of electronic energies, we performed single-point energy calculations using the M06-D3/LACVP++** method. For all stationary points, we performed solvation calculations using the Poisson−Boltzmann self-consistent polarizable continuum method as implemented in the Jaguar 9.5 software (Schrodinger 2017) to represent the toluene (dielectric constant equals 2.379 and the effective radius of 2.762 Å). All energies discussed in this work are Gibbs free energies defined as the sum of electronic energy, solvation energy, thermal correction to enthalpy, zero-point energy correction, and the negative product of temperature and entropy at 298 K.

In the noncovalent interaction (NCI) analysis, we used the B3LYP-optimized structures. The wavefuctions needed for the analysis were obtained from Gaussian 09,[44] single-point calculations using M06-D3/6−311++G(d,p) for C, H, N, P, O and M06-D3/LANL2DZ for Ru for all stationary points. The final analysis was carried out with Multiwfn ver 3.6.[45] The analysis of results included generation of isosurface plots (see Supporting Information) and visualization of weak interactions.

Calculations using the DLPNO-CCSD approach were performed using Orca 4.0.[46] The results are presented in Supporting Information (Scheme S1). We performed single-point calculations using def2-svp and def2/J basis sets.[47]

Calculation associated with intramolecular interactions based on symmetry-adapted perturbation theory (SAPT) was performed using the Psi4 software.[48] We used the F-SAPT/jun-cc-pVDZ level of theory and SAPT2+3/jun-cc-pVDZ level of theory. The results of these calculations are presented in detail in the Supporting Information (Table S5).

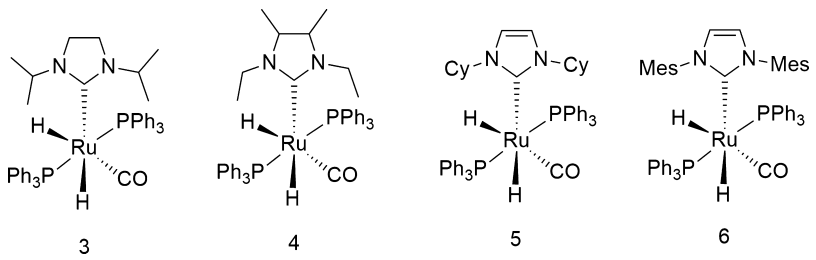

Figure 3. New ruthenium-based catalysts studied in this work as potential catalysts for the hydrogenation of ethylene and ruthenacyclization.

https://dx.doi.org/10.1021/acs.jpca.0c01354
J. Phys. Chem. A 2020, 124, 3609−3617

Scheme 1. Gibbs Free Energy Profile for the Ethylene Hydrogenation[a]

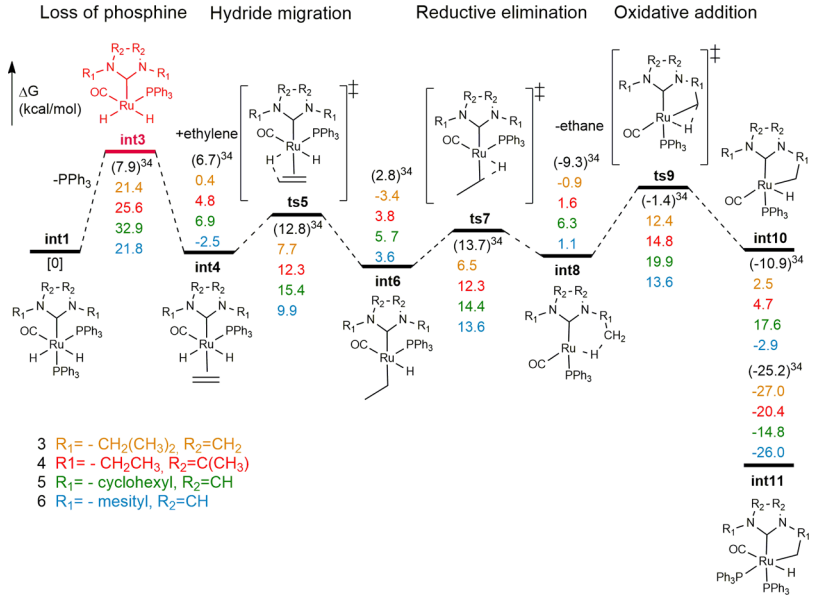

[a]Gibbs free energy values (M06-D3/LACVP++**) are given in kcal/mol, for four investigated complexes.

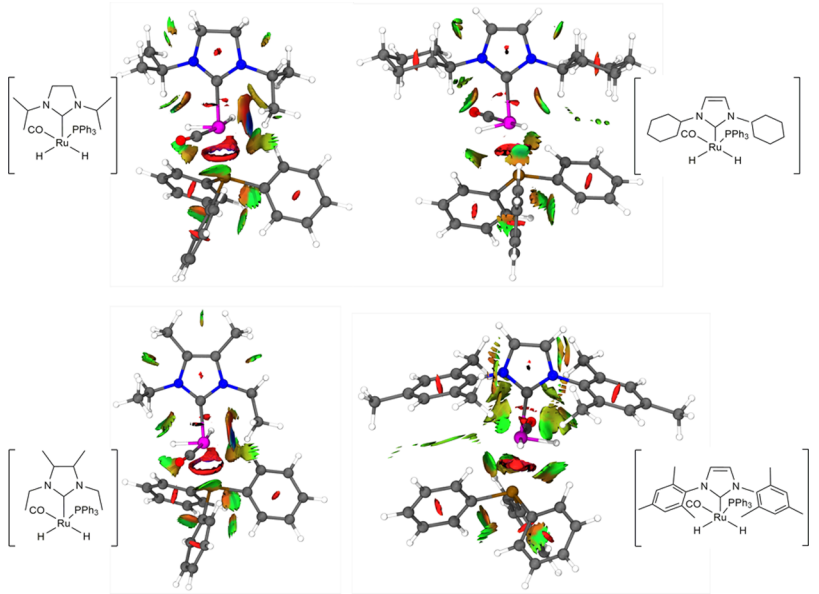

Figure 4. Optimized structures of **int3** with visualized weak interactions regions. Blue color corresponds to strong attraction, green corresponds to van der Waals interaction, and red corresponds to steric effects in rings.

Considering the accuracy of obtained Gibbs free energy value, we decided to reevaluate the thermochemical contributions. The Gibbs free energies reported in the manuscript used the quasi-rigid-rotor harmonic oscillator (quasi-RRHO) approximation. We additionally reevaluated the entropic and enthalpic contributions of low frequency modes below 100 cm^{-1} using the previously reported Grimme[49] and Cramer/Truhlar[50] models in the GoodVibes[51] software. The results using these different approaches were, however, similar and did not alter the conclusions. Therefore, we decided to base our discussion on the results with quasi-RRHO approximation, while the detailed results from these calculations are presented in Table S3 (Supporting Information).

RESULTS AND DISCUSSION

We investigated the mechanism of the tandem alkene hydrogenation with intramolecular C−H activation reaction with catalysts **1** and **3**−**6**. For all complexes, we considered dissociative reactive pathway proposed by the Whittlesey group,[30] which consists of stepwise olefin association, hydride migration, reductive elimination, and oxidative addition via the Ru(0) intermediate. Within this mechanism, Houk et al. identified two crucial steps which may be rate-limiting for the entire catalytic cycle irrespective of the olefin or the catalysts used; these are the hydride migration and reductive elimination. In his DFT calculations, however, the catalytic cycle initiates with the dissociation of the PPh_3 moiety from **1** with the Gibbs free energy of dissociation estimated at 7.9 kcal/mol. This value

https://dx.doi.org/10.1021/acs.jpca.0c01354
J. Phys. Chem. A 2020, 124, 3609−3617

may seem rather surprisingly low considering that very well-known olefin metathesis ruthenium catalysts also activate via phosphine dissociation, but their experimentally measured phosphine dissociation free energies are in the 19−23 kcal/mol range.[52,53] While one may argue whether Grubbs complexes and **1** are genuinely that similar, such a difference is striking and we decided to make additional calculations to verify this problem and obtain the best possible estimate of this value. For complex **1**, we obtained the following values: 13.5 kcal/mol using M06 functional and 21.1 kcal/mol using the DLPNO-CCSD(T) approach (Scheme S1, Supporting Information). For the remaining investigated catalysts **3**−**6**, we also obtained values in the 21−32 kcal/mol range using the M06 method (Scheme 1). All of these results are much closer to the expected range of 19−23 kcal/mol and, in our opinion, are much more accurate estimates of the Gibbs free energies of $-PPh_3$ dissociation. It is also an important result from the catalytic cycle point of view because the obtained 13.5 kcal/mol value for **1** is close to the suggested barriers of the rate-limiting steps of this reaction, estimated by Houk and co-workers at 13−20 kcal/mol. As a result for **1** as well as all complexes studied in this work, we may need to consider the phosphine dissociation as another candidate for the rate-limiting step of this reaction, similarly to the initiation of the Grubbs and Grubbs-like catalysts in olefin metathesis.[52,54,55]

Scheme 1 displays the calculated Gibbs free energy profile of the catalytic cycle with ethylene as a substrate for all investigated complexes. The catalytic cycle consists of four steps: (1) exchange of phosphine ligand for ethylene, (2) hydride migration, (3) reduction and elimination of ethane, and (4) oxidative addition and creation of the ruthenacycle product (**int10**). In the first step of the catalytic cycle, the dissociation of the PPh_3 group forms intermediates **int3-3**, **int3-4**, **int3-5**, and **int3-6**, respectively, which are less stable than precatalyst **int1** for each investigated carbene by more than 20 kcal/mol. Because of the highest Gibbs free energy (ΔG) barrier in the entire catalytic cycle, the loss of phosphine is the rate-limiting step for all investigated catalysts. Also, for all considered catalysts, the ΔG with respect to precatalyst **int1** is similar and exceeds the value of 20 kcal/mol, but for **int3-5**, it is significantly higher and reaches more than 30 kcal/mol. To explain this phenomenon, we performed NCI analysis (see Figure 4).[56] NCI is a helpful technique for description of van der Waals interactions, repulsive steric interactions, and hydrogen bonds, where the type and strength of these interactions can be examined through RDG (Reduced Density Gradient) surface analysis and topological properties of electron density $\rho(r)$ at the (3, −1) and (3, +1) critical points (CPs), corresponding to bond and ring CPs, respectively.[57−60]

The NHCs used in our study differ in electronic properties, resulting in significant differences in intramolecular interactions within each catalyst (Figure 4). To reveal the nature of these interactions, we performed the topological analysis and NCI investigation for the rate-limiting step (**int3**) and all transition states (**ts5**, **ts7**, and **ts9**). We analyzed the electron density, sign of the second largest eigenvalue of the Laplacian of electron density and potential energy density at the CPs corresponding to these interactions (Tables S7 and S8, Supporting Information). In addition, for each NHCs, we decided to separate the different thermodynamic contributions to the Gibbs free energy differences between individual intermediates (Table 1).

For **int3**, the highest energetic barrier (32.9 kcal/mol) was found in **int3-5**. We noticed that it arises mainly from the rise in electronic energy (ΔE) and quite low entropy gain (ΔS). On the other hand, the lowest barrier of ΔG is observed for **int3-3** and **int3-6** (21.4 and 21.8 kcal/mol, respectively). Compared to **int3-5**, the increase in electronic energy is lower and the entropy rise is significantly higher for these compounds.

Further, we attempted to seek for correlations between the electronic energy and intramolecular interactions of considered complexes. We noticed more than six (3,−1) CPs for intermediates: **int3-3**, **int3-4**, and **int3-6** while for **int3-5**-, only three CPs localized were noticed between NHCs and phosphine part (Table S6, Supporting Information), suggesting that **int3-5** is less stabilized. Interestingly, all described CPs showed similar topology properties, except CPs 67 and 68 for **int3-3** and **int3-4**, respectively (Tables S6 and S7, Supporting Information). These CPs correspond to interactions between Ru and H from the N-substituent (ethyl and isopropyl). For these CPs, the Laplacian of electron density is considerably higher and the potential energy density is lower by an order of magnitude than for the other CPs. It indicates that these interactions are additional stabilization for considered complexes. Other intramolecular interactions exhibit properties characteristic for weak van der Waals interactions. Interestingly, for intermediate **int3-6** bearing the mesityl substituents, we have observed van der Waals interaction (the green sphere in Figure 4) between the mesityl ring and one of the benzene rings of the phosphine. Furthermore, for **int3-5**, there is an arene-sp^2 CH_2 type interaction between the benzene ring of the phosphine and

Table 1. Values of ΔS (Entropy), ΔH (Enthalpy), ΔE (Electronic Energy), and ΔG (Gibbs Free Energy) for All Investigated Catalysts 3, 4, 5, and 6 in int3, ts5, ts7, and ts9[a]

	catalyst	int3	ts5	ts7	ts9
ΔS	3	56.9	13.4	23.0	55.0
ΔH		0.1	−0.6	0.1	−0.4
ΔE		38.4	12.1	12.2	25.9
ΔG		21.4	7.7	6.5	12.4
		int3	ts5	ts7	ts9
ΔS	4	49.0	4.5	10.7	48.2
ΔH		−0.3	−1.5	−1.0	−1.0
ΔE		42.0	15.6	15.8	27.7
ΔG		25.6	12.3	12.3	14.8
		int3	**ts5**	**ts7**	**ts9**
ΔS	5	49.9	7.5	16.4	47.3
ΔH		−0.5	−1.1	−0.5	−0.8
ΔE		49.3	18.7	18.8	32.0
ΔG		32.9	15.4	14.4	19.9
		int3	**ts5**	**ts7**	**ts9**
ΔS	6	60.3	15.7	10.3	56.4
ΔH		0.2	−0.9	−1.5	−0.4
ΔE		40.1	16.1	17.3	28.1
ΔG		21.8	9.9	13.6	13.6

[a]All values are given in kcal/mol.

Table 2. Value of the Ru−C−N Angle for ts7 and int8 after Dissociation of Ethane

catalyst	angle value for **ts7**	angle value for **int8**
1	123.8[34]	119.8[34]
3	122.5	118.9
4	124.7	120.7
5	124.3	123.2
6	124.7	122.4

https://dx.doi.org/10.1021/acs.jpca.0c01354
J. Phys. Chem. A 2020, 124, 3609−3617

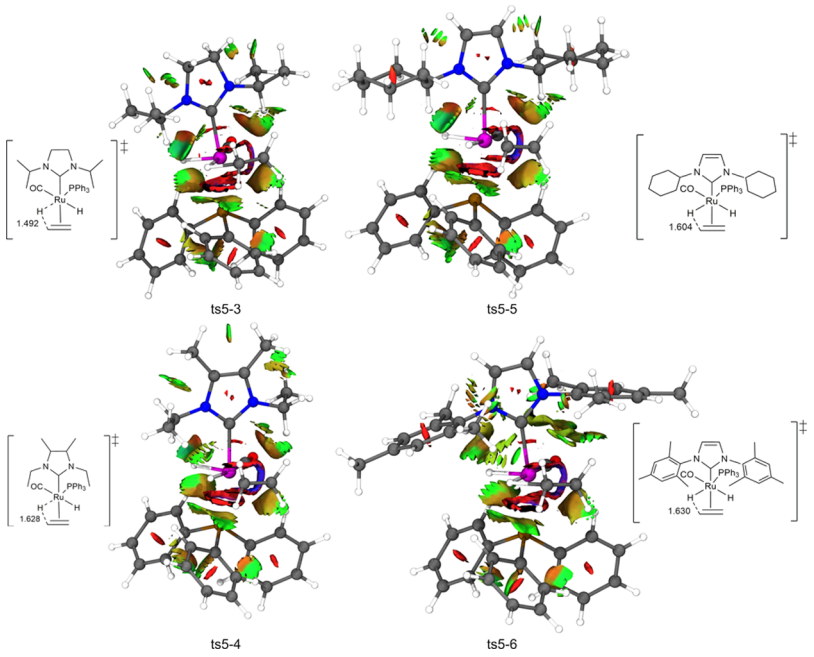

Figure 5. Visualization of weak interaction region of the **ts5** transition states. Bond lengths are given in Å. The isosurface value are represented by colors: blue corresponds to strong attraction, green corresponds to van der Waals interaction, and red corresponds to steric effects in rings.

cyclohexane substituent. Although this type of interactions is usually weaker than classical H-bonding,[61] here it significantly affects the geometry of this intermediate.

In the case of **int3-5**, the phosphine ligand is substantially rotated along the main axis of symmetry relative to **int3-3** and **int3-4**. The rotation of the molecule is a result of uneven distribution of electron density around the ruthenium center. Similar features in geometry are present in the case of intermediate **int3-6**, but they are a result of $\pi-\pi$ interactions between the benzene ring of phosphine and the N-substituted mesityl ring. Analogous types of interactions can be also observed between ethyl N-substituent and one of the benzene rings in intermediate **int3-4**. Considering the steric interactions in investigated complexes, we also analyzed (3,+1) CPs. Similarly to bond CPs, we noticed more than six CPs for **int3-3**, **int3-4**, and **int3-6**, whereas for less stabilized **int3-5**, we observed only four CPs in the same part of compounds. Interestingly, the (3,+1) and (3,−1) CPs are grouped in pairs. Most of the steric hindrance is located between ruthenium and phosphorus atoms. The Laplacian of electron density and potential energy density for all intermediates show similar values at these (3,+1) CPs, which suggests that steric interactions in the complexes are of comparable strength for these step.

Moreover, within the phosphine ligand between the phenyl rings, we found additional pairs of (3,−1) and (3,+1) CPs, two for **int3-4** and **int3-6** and three for **int3-3**. For **int3-5**, none of the CPs was found within this space. This implies that the phosphine part is worse stabilized in **int3-5** compared to the other complexes, which may propagate into the highest Gibbs free energy of this compound. Conversely, the phosphine in **int3-3** is probably the most optimally stabilized which may translate into the lowest Gibbs free energy of this complex.

In the next step of the catalytic cycle, the ethylene (olefin) association occurs. This process stabilizes the complex, which results in significantly lower energetic state. The resulting complex **int4** is an octahedral intermediate which shows lower stability for carbenes with cyclohexyl and ethyl N-substituents. We observed for **int4-5** more noncovalent interactions than in previous intermediate **int3-5** which was a result of association of ethylene. This step is followed by hydride migration from the complex to ethylene (olefin) in which 16-electron intermediate **int6** via transition-state **ts5** is formed. The energy required for C−H reductive elimination, being a difference between **int4** and **ts5**, is about 6−12 kcal/mol, which is consistent with the results obtained by Houk et al.[34] The release of ethylene is preceded by the migration of the two hydrogen atoms from the ruthenium complex. One of the hydride ligands is transferred to the ethylene in the **ts5**. For complex **ts5-6**, the energy required for transfer of the hydrogen is relatively high being more than 12 kcal/mol compared to **int4-6** (9.9 kcal/mol with respect to the precatalyst), while for **ts5-3** and **ts5-4**, the energy barriers are merely 7 kcal/mol in relation to the **int3-3** and **int3-4** (7.7 and 12.3 kcal/mol with respect to precatalyst). Despite the minor differences in the geometry of the associated ethylene molecule, the Gibbs free energies are significantly different for the **ts5** states. For **ts5-3** and **ts5-6** as in previously analyzed **int3**, the lowest electronic energy (ΔE) is related to the lowest Gibbs free energy (7.7 and 9.9 kcal/mol, respectively) and occurs simultaneously with the highest entropy gain for these complexes (13.4 and 15.7 kcal/mol, respectively). It appears, however, that the differences in ΔG value in **ts5** are mainly dictated by entropy contribution.

The lowest electronic energy observed for **ts5-3** may relate to the greater interaction with ethylene which is reflected in the shorter distance between the migrating hydride and ethylene (1.49 Å) in comparison with other **ts5** geometries, with distances exceeding 1.6 Å. Also, we noticed that the CP located between ethylene and the ruthenium center in **ts5-3** is characterized by the most negative value of energy density (Table S8, Supporting Information) (−0.0139 a.u.). The other weak intramolecular interactions within the **ts5-3** between the phosphine and NHC ligand also seem to stabilize the molecule stronger than for the other complexes (Figure 5). All **ts5** transition states display significant steric effects around the

https://dx.doi.org/10.1021/acs.jpca.0c01354
J. Phys. Chem. A 2020, 124, 3609−3617

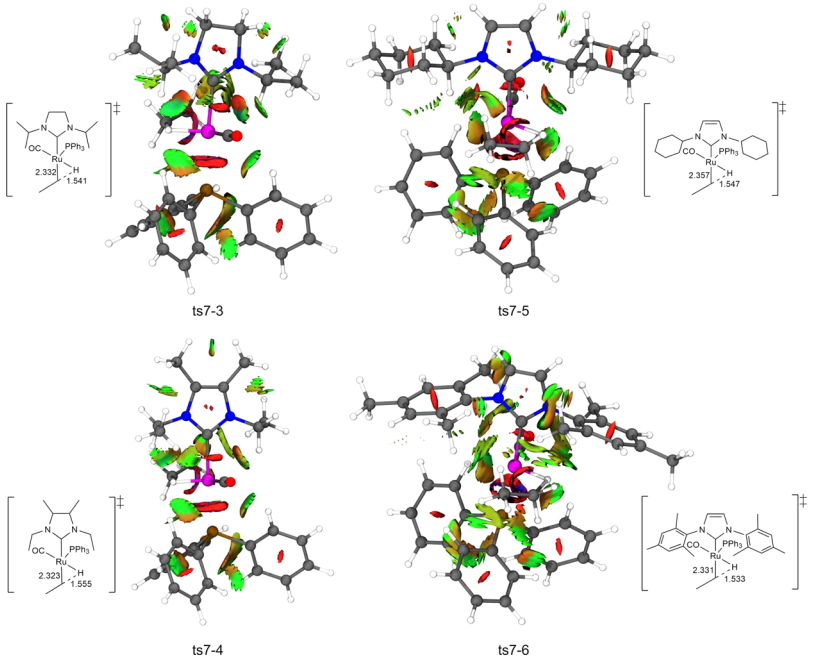

Figure 6. Visualization of weak interaction region of the **ts7** transition states. Bond lengths are given in Å. The isosurface value are represented by colors: blue corresponds to strong attraction, green corresponds to van der Waals interaction, and red corresponds to steric effects in rings.

ruthenium center because of the presence of the associated ethylene molecule. The energy of density associated with these interactions roughly reflect the electronic energy differences between the **ts5** complexes. Intriguingly, for the transition from **int3-5** to **ts5-5**, we noticed the largest increase in the number of CPs, associated with the addition of ethylene (Tables S7 and S8 in Supporting Information). This corresponds to the most significant decrease in the Gibbs free energy (17.5 kcal/mol between **int3-5** and **ts5-5**).

Additionally, we also examined the intramolecular interaction using SAPT. The F-SAPT module allows us to compute the interaction between two parts of moieties in one molecule[62] and is useful over complicated intramolecular interactions. For **ts5** transition states, we have performed additional analysis based on SAPT2 + 3 and SAPT0 results (Supporting Information, Table S5). We considered interaction between N-substituents and associated ethylene, benzenes from the phosphine group and associated ethylene, and interaction between N-substituents and the phosphine ligand. In most cases, we noticed values of SAPT2+3 and SAPT0 lower than −0.5 kcal/mol, regardless of the type of catalysts or interacting part of molecules. As a consequence, these results are inconclusive because of very small interaction energies. Only for **ts5-6**, we observed stronger interaction between the phosphine ligand and N-substituents than for other transition states (values higher than 0.5 kcal/mol).

The transfer of the second hydride ligand is concomitant with the dissociation of ethane moiety in the **ts7** transition state. We found that the energy barriers in **ts7** are between 8.5 kcal/mol (for **ts7-4**) and 9.9 kcal/mol (for **ts7-3**) with respect to the previous intermediate **int6-3** and **int6-4** (6.5 kcal for **ts7-3** and 12.3 kcal/mol for **7ts-4** with respect to the precatalyst **int1-3** and **int1-4**, respectively). Three of the **ts7** are characterized by the Gibbs free energy value ranging from 12.3 to 14.4 kcal/mol (**ts7-4**, **ts7-5**, and **ts7-6**), while the highest value of ΔG is featured by **ts7-5**. Similarly to the previous transition state, the highest entropy and the lowest electronic energy occurs for **ts7-3** (23.0 and 12.2 kcal/mol, respectively). This translates into the lowest Gibbs free energy in **ts7**. On the other hand, the highest Gibbs free energy of **ts7-5** results from the most positive electronic energy.

For **ts7** transition states, we observed many weak van der Waals interactions between the NHC ligand and phosphine part as well as between this moieties and ethane (see Figure 6). Similar to the intermediate **int3-5**, for **ts7-5**, we have also detected the sp^2 CH_2−arene interactions, which manifest as weak van der Waals interactions. Compared to **ts5**, we noticed smaller steric interactions associated with the release of the ethane.

Among the CPs (3,−1) and (3,+1) type for **ts7** for all considered catalysts, we did not observe significant changes in value of topological properties (Laplacian of electron density and the energy of electron density). Therefore, it is hard to find the clear correlation between the electronic energy differences and the stabilizing/destabilizing interactions within this transition state.

The loss of ethane initiates the next step of the catalytic cycle, namely, the oxidative addition to the C−H bond of the carbene N-substituent to form the ruthenacycle product. In the newly created intermediate **int8**, one can observe gentle changes in the Ru−C−N angle value. Compared to the previous transition state, **ts7**, these angles' values differ by at least 2° (see Figure 7, Table 2) and are accompanied by a slight rotation of one of the N-substituents.

This rotation becomes significant during C−H activation. The creation of the stable product (**int10-3**, **int10-4**, **int10-5**, and **int10-6**) is preceded by the transition state **ts9** and requires a relatively high energy of more than 12.0 kcal/mol for all catalysts (related to the **int1**). The formation of the Ru− C bond is accompanied by a steric hindrance between the N-substituent and the ruthenium core of the molecule. For **ts9-5**, during the N-substituent rotation, we have also observed stronger van der Waals interactions between the cyclohexane group and phosphine's benzene rings. Moreover, for this transition state,

https://dx.doi.org/10.1021/acs.jpca.0c01354
J. Phys. Chem. A 2020, 124, 3609−3617

we noticed that the cyclohexyl group is the most rotated one relative to the reference position from **int1-5**, which corresponds to the highest energetic barrier (19.9 kcal/mol). The highest free energy barrier can be also related to the result first described by Bloom and Wheeler. They have shown that the interaction between benzenes dimer is weaker than interaction between cyclohexane and benzene.[63] For intermediate with the cyclohexane substituent, we observed the free Gibbs energy barrier higher of more than 6 kcal/mol with respect to the transition state of complex with the mesityl substituent. We presume that this situation may be a result of the fact that breaking the interaction between cyclohexyl and benzene (**ts9-5**) requires more energy than breaking the interactions between two aromatic components (**ts9-6**). For **ts9-5**, the highest Gibbs free energy arises not only from the highest electronic energy but also from the lowest entropy gain among the considered complexes. On the other hand, the **ts9-3** possess the most favorable electronic energy and entropy contribution, which results in the lowest ΔG value.

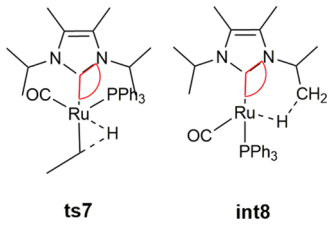

Figure 7. Definition of the Ru−C−N angle in **ts7** and **int8**.

For **ts9** (Figure 8), the complexes with bulky N-substituents (mesityl and cyclohexyl), we observed more CPs (six) between the NHC ligand and other part of the compound than for others catalysts (**ts9-3** and **ts9-4**, four and three, respectively). However surprisingly, the electronic energy of these complexes is the least favorable. Furthermore, exploring the (3,−1) CPs for **ts9-4**, we observed CP with the negative value of Laplacian of electron density. It is localized between the newly created Ru−C bond and the H atom simultaneously migrating from that carbon to the ruthenium. Moreover, the amount of (3,+1) CPs is the same for **ts9-3**, **ts9-5**, and **ts9-6** (six CPs), while only three CPs were found for **ts9-4**. For one of the CPs in **ts9-3**, localized between the hydrogen atom and newly created Ru−C bond, we observed a high value of Laplacian of electron density and hence the negative energy density. This suggests the stabilizing character of this interaction, which propagates into the lowest electronic energy in this state.

In the final step of the cycle, the phosphine ligand, which dissociated in the first step, can associate back to the complex after the reductive elimination step.[34] This leads to the creation of more stable complex **int11** [four-coordinate Ru (0)], which ends the catalytic cycle.

CONCLUSIONS

Inspired by computational results of Houk and co-workers, who studied the mechanism of olefin hydrogenation with simultaneous activation of the C−H bond, we expanded upon their work to gain more mechanistic insights into this reaction. We studied the same reaction with four catalysts bearing NHCs with different electronic and steric properties.

Our calculations indicate that contrary to the previous computational results, the dissociation of the phosphine from the precatalyst may be the rate-limiting step of the entire catalytic cycle for catalysts **3**−**6**. We also show that this reaction favors catalysts bearing NHCs with aliphatic and aromatic side groups. Moreover cyclohexyl-substituted NHC is predicted to have high energy barriers for most reactions in the catalytic cycle. Our noncovalent interaction analysis reveals crucial interactions which stabilize/destabilize important intermediates and transition states in this reaction. We show that during the design of new, potential catalysts, the specific noncovalent interactions should also be considered. Even though their individual input into the interaction energies between various parts of catalysts is on the level of 0.5−3 kcal/mol,[64] collectively, they are important for catalyst reactivity and stability, giving rise to relatively large differences in the final energy barriers of transition states.

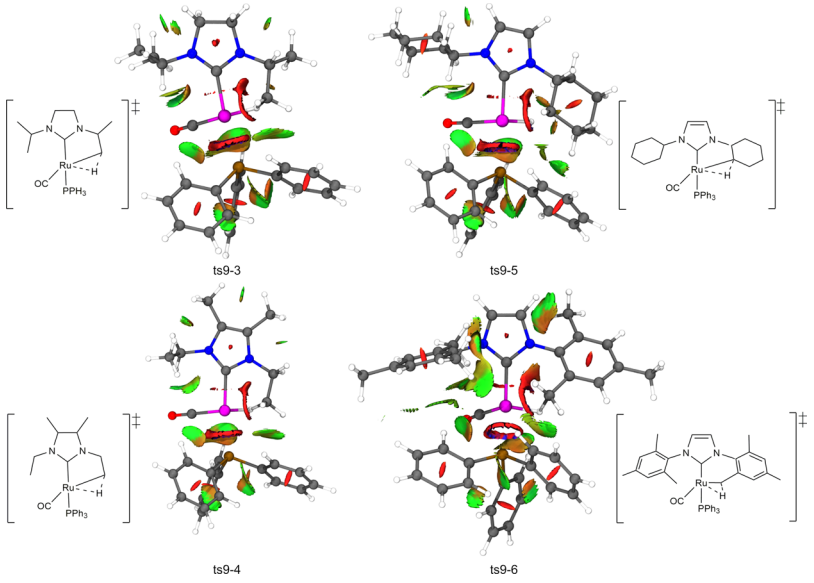

Figure 8. Visualization of weak interaction region of the **ts9** transition state. The isosurface values are represented by colors: blue corresponds to strong attraction, green corresponds to van der Waals interaction, and red corresponds to steric effects in rings.

https://dx.doi.org/10.1021/acs.jpca.0c01354
J. Phys. Chem. A 2020, 124, 3609−3617

■ ASSOCIATED CONTENT

Supporting Information

The Supporting Information is available free of charge at https://pubs.acs.org/doi/10.1021/acs.jpca.0c01354.

M06 and CCSD-DLPNO Gibbs free energy profile for the ethylene hydrogenation for catalyst **1**, total energy values (E) and Gibbs free energy values (ΔG as defined in the manuscript) for catalysts **1**, **3**, **4**, **5**, **6**, and its complexes, RDG effective density plots and the CPs (3,−1) and (3, +1) and its characterization for intermediate **int3** and transition state **ts5**, **ts7**, and **ts9** for every considered catalysts (**3**, **4**, **5**, and **6**) (PDF)

Coordination of all intermediates and transition states (XYZ)

■ AUTHOR INFORMATION

Corresponding Authors

Katarzyna Młodzikowska-Pieńko − *Centre of New Technologies and Faculty of Chemistry, University of Warsaw, 02-097 Warsaw, Poland*; Email: k.mlodzikowska@cent.uw.edu.pl

Bartosz Trzaskowski − *Centre of New Technologies, University of Warsaw, 02-097 Warsaw, Poland*; orcid.org/0000-0003-2385-1476; Email: trzask@cent.uw.edu.pl

Complete contact information is available at: https://pubs.acs.org/10.1021/acs.jpca.0c01354

Author Contributions

The manuscript was written through contributions of all authors. All authors have given approval to the final version of the manuscript.

Notes

The authors declare no competing financial interest.

■ ACKNOWLEDGMENTS

We acknowledge research support from the National Science Centre grants UMO-2016/22/E/ST4/00573.

■ REFERENCES

(1) Arduengo, A. J.; Harlow, R. L.; Kline, M. A Stable Crystalline Carbene. *J. Am. Chem. Soc.* **1991**, *113*, 361−363.

(2) Bourissou, D.; Guerret, O.; Gabbaï, F. P.; Bertrand, G. Stable Carbenes. *Chem. Rev.* **2000**, *100*, 39−92.

(3) Díez-González, S.; Marion, N.; Nolan, S. P. N-Heterocyclic Carbenes in Late Transition Metal Catalysis. *Chem. Rev.* **2009**, *109*, 3612−3676.

(4) Fèvre, M.; Pinaud, J.; Gnanou, Y.; Vignolle, J.; Taton, D. N-Heterocyclic Carbenes (NHCs) as Organocatalysts and Structural Components in Metal-Free Polymer Synthesis. *Chem. Soc. Rev.* **2013**, *42*, 2142−2172.

(5) Bugaut, X.; Glorius, F. Organocatalytic Umpolung: N-Heterocyclic Carbenes and Beyond. *Chem. Soc. Rev.* **2012**, *41*, 3511−3522.

(6) Flanigan, D. M.; Romanov-Michailidis, F.; White, N. A.; Rovis, T. Organocatalytic Reactions Enabled by N-Heterocyclic Carbenes. *Chem. Rev.* **2015**, *115*, 9307−9387.

(7) Vougioukalakis, G. C.; Grubbs, R. H. Ruthenium-Based Heterocyclic Carbene-Coordinated Olefin Metathesis Catalysts. *Chem. Rev.* **2010**, *110*, 1746−1787.

(8) Samojłowicz, C.; Bieniek, M.; Grela, K. Ruthenium-Based Olefin Metathesis Catalysts Bearing N-Heterocyclic Carbene Ligands. *Chem. Rev.* **2009**, *109*, 3708−3742.

(9) Urbina-Blanco, C. A.; Poater, A.; Lebl, T.; Manzini, S.; Slawin, A. M. Z.; Cavallo, L.; Nolan, S. P. The Activation Mechanism of Ru−Indenylidene Complexes in Olefin Metathesis. *J. Am. Chem. Soc.* **2013**, *135*, 7073−7079.

(10) Nelson, D. J.; Manzini, S.; Urbina-Blanco, C. A.; Nolan, S. P. Key Processes in Ruthenium-Catalysed Olefin Metathesis. *Chem. Commun.* **2014**, *50*, 10355−10375.

(11) Schwartsburd, L.; Whittlesey, M. K. Ruthenium N-Heterocyclic Carbene Complexes for the Catalysis of Nonmetathesis Organic Transformations. *N-Heterocyclic Carbenes* **2014**, *9*, 341−370.

(12) Noyori, R.; Ohkuma, T. Asymmetric Catalysis by Architectural and Functional Molecular Engineering: Practical Chemo- and Stereoselective Hydrogenation of Ketones. *Angew. Chem. Int. Ed.* **2001**, *40*, 40−73.

(13) Wang, D.; Astruc, D. The Golden Age of Transfer Hydrogenation. *Chem. Rev.* **2015**, *115*, 6621−6686.

(14) Lee, H. M.; Smith, D. C.; He, Z.; Stevens, E. D.; Yi, C. S.; Nolan, S. P. Catalytic Hydrogenation of Alkenes by the Ruthenium−Carbene Complex HRu(CO)Cl(PCy3)(IMes) (IMes = Bis(1,3-(2,4,6-Trimethylphenyl)Imidazole-2-Ylidene). *Organometallics* **2001**, *20*, 794−797.

(15) Edwards, M. G.; Jazzar, R. F. R.; Paine, B. M.; Shermer, D. J.; Whittlesey, M. K.; Williams, J. M. J.; Edney, D. D. Borrowing Hydrogen: A Catalytic Route to C−C Bond Formation from Alcohols. *Chem. Commun.* **2004**, *1*, 90−91.

(16) Burling, S.; Mahon, M. F.; Paine, B. M.; Whittlesey, M. K.; Williams, J. M. J. Reversible Intramolecular Alkyl C−H Bond Activation, Alcohol Dehydrogenation, and Trans−Cis Dihydride Isomerization in Ruthenium N-Heterocyclic Carbene Complexes. *Organometallics* **2004**, *23*, 4537−4539.

(17) Dharmasena, U. L.; Foucault, H. M.; dos Santos, E. N.; Fogg, D. E.; Nolan, S. P. N-Heterocyclic Carbenes as Activating Ligands for Hydrogenation and Isomerization of Unactivated Olefins. *Organometallics* **2005**, *24*, 1056−1058.

(18) Lee, J. P.; Ke, Z.; Ramírez, M. A.; Gunnoe, T. B.; Cundari, T. R.; Boyle, P. D.; Petersen, J. L. Six-, Five-, and Four-Coordinate Ruthenium(II) Hydride Complexes Supported by N-Heterocyclic Carbene Ligands: Synthesis, Characterization, Fundamental Reactivity, and Catalytic Hydrogenation of Olefins, Aldehydes, and Ketones. *Organometallics* **2009**, *28*, 1758−1775.

(19) Wang, T.; Pranckevicius, C.; Lund, C. L.; Sgro, M. J.; Stephan, D. W. Ruthenium Carbene−Diether Ligand Complexes: Catalysts for Hydrogenation of Olefins. *Organometallics* **2013**, *32*, 2168−2177.

(20) Crabtree, R. H.; Lei, A. Introduction: CH Activation. *Chem. Rev.* **2017**, *117*, 8481−8482.

(21) Stoutland, P. O.; Bergman, R. G.; Nolan, S. P.; Hoff, C. D. The Thermodynamic Driving Force for C—H Activation at Iridium. *Polyhedron* **1988**, *7*, 1429−1440.

(22) Labinger, J. A. Platinum-Catalyzed C−H Functionalization. *Chem. Rev.* **2017**, *117*, 8483−8496.

(23) He, J.; Wasa, M.; Chan, K. S. L.; Shao, Q.; Yu, J.-Q. Palladium-Catalyzed Transformations of Alkyl C−H Bonds. *Chem. Rev.* **2017**, *117*, 8754−8786.

(24) Shang, R.; Ilies, L.; Nakamura, E. Iron-Catalyzed C−H Bond Activation. *Chem. Rev.* **2017**, *117*, 9086−9139.

(25) Newton, C. G.; Wang, S.-G.; Oliveira, C. C.; Cramer, N. Catalytic Enantioselective Transformations Involving C−H Bond Cleavage by Transition-Metal Complexes. *Chem. Rev.* **2017**, *117*, 8908−8976.

(26) Gensch, T.; Hopkinson, M. N.; Glorius, F.; Wencel-Delord, J. Mild Metal-Catalyzed C−H Activation: Examples and Concepts. *Chem. Soc. Rev.* **2016**, *45*, 2900−2936.

(27) Arockiam, P. B.; Bruneau, C.; Dixneuf, P. H. Ruthenium(II)-Catalyzed C−H Bond Activation and Functionalization. *Chem. Rev.* **2012**, *112*, 5879−5918.

(28) Huang, J.; Stevens, E. D.; Nolan, S. P. Intramolecular C−H Activation Involving a Rhodium−Imidazol-2-Ylidene Complex and Its Reaction with H2 and CO. *Organometallics* **2000**, *19*, 1194−1197.

(29) Zhao, Q.; Meng, G.; Nolan, S. P.; Szostak, M. N-Heterocyclic Carbene Complexes in C−H Activation Reactions. *Chem. Rev.* **2020**, *120*, 1981−2048.

(30) Burling, S.; Paine, B. M.; Nama, D.; Brown, V. S.; Mahon, M. F.; Prior, T. J.; Pregosin, P. S.; Whittlesey, M. K.; Williams, J. M. J. CH Activation Reactions of Ruthenium N-Heterocyclic Carbene Complexes: Application in a Catalytic Tandem Reaction Involving CC Bond Formation from Alcohols. *J. Am. Chem. Soc.* **2007**, *129*, 1987−1995.
(31) Häller, L. J. L.; Page, M. J.; Macgregor, S. A.; Mahon, M. F.; Whittlesey, M. K. Activation of an Alkyl C−H Bond Geminal to an Agostic Interaction: An Unusual Mode of Base-Induced C−H Activation. *J. Am. Chem. Soc.* **2009**, *131*, 4604−4605.
(32) Diggle, R. A.; Macgregor, S. A.; Whittlesey, M. K. Computational Study of C−C Activation of 1,3-Dimesitylimidazol-2-Ylidene (IMes) at Ruthenium: The Role of Ligand Bulk in Accessing Reactive Intermediates. *Organometallics* **2008**, *27*, 617−625.
(33) Diggle, R. A.; Kennedy, A. A.; Macgregor, S. A.; Whittlesey, M. K. Computational Studies of Intramolecular Carbon−Heteroatom Bond Activation of N-Aryl Heterocyclic Carbene Ligands. *Organometallics* **2008**, *27*, 938−944.
(34) Wenz, K. M.; Liu, P.; Houk, K. N. Intramolecular C − H Activation Reactions of Ru(NHC) Complexes Combined with H 2 Transfer to Alkenes: A Theoretical Elucidation of Mechanisms and Effects of Ligands on Reactivities. *Organometallics* **2017**, *2*, 3613.
(35) Małecki, P.; Gajda, K.; Gajda, R.; Woźniak, K.; Trzaskowski, B.; Kajetanowicz, A.; Grela, K. Specialized Ruthenium Olefin Metathesis Catalysts Bearing Bulky Unsymmetrical NHC Ligands: Computations, Synthesis, and Application. *ACS Catal.* **2019**, *9*, 587−598.
(36) Jawiczuk, M.; Janaszkiewicz, A.; Trzaskowski, B. The Influence of the Cationic Carbenes on the Initiation Kinetics of Ruthenium-Based Metathesis Catalysts; a DFT Study. *Beilstein J. Org. Chem.* **2018**, *14*, 2872−2880.
(37) Jolly, P. I.; Marczyk, A.; Małecki, P.; Ablialimov, O.; Trzybiński, D.; Woźniak, K.; Osella, S.; Trzaskowski, B.; Grela, K. Azoliniums, Adducts, NHCs and Azomethine Ylides: Divergence in Wanzlick Equilibrium and Olefin Metathesis Catalyst Formation. *Chem.—Eur. J.* **2018**, *24*, 4785−4789.
(38) Grudzień, K.; Trzaskowski, B.; Smoleń, M.; Gajda, R.; Woźniak, K.; Grela, K. Hoveyda−Grubbs Catalyst Analogues Bearing the Derivatives of N-Phenylpyrrol in the Carbene Ligand − Structure, Stability, Activity and Unique Ruthenium−Phenyl Interactions. *Dalton Trans.* **2017**, *46*, 11790−11799.
(39) Ambrosio, C.; Paradiso, V.; Costabile, C.; Bertolasi, V.; Caruso, T.; Grisi, F. Stable Ruthenium Olefin Metathesis Catalysts Bearing Symmetrical NHC Ligands with Primary and Secondary N-Alkyl Groups. *Dalton Trans.* **2018**, *47*, 6615−6627.
(40) Burling, S.; Mas-Marzá, E.; Valpuesta, J. E. V.; Mahon, M. F.; Whittlesey, M. K. Coordination, Agostic Stabilization, and C−H Bond Activation of N-Alkyl Heterocyclic Carbenes by Coordinatively Unsaturated Ruthenium Hydride Chloride Complexes. *Organometallics* **2009**, *28*, 6676−6686.
(41) Ledger, A. E. W.; Mahon, M. F.; Whittlesey, M. K.; Williams, J. M. J. J. [Ru(NHC)(Xantphos)(CO)H2] Complexes: Intramolecular C−H Activation and Applications in C−C Bond Formation. *Dalton Trans.* **2009**, *35*, 6941−6947.
(42) Chilvers, M. J.; Jazzar, R. F. R.; Mahon, M. F.; Whittlesey, M. K. Reversible CH Bond Activation Reactions of the N-Heterocyclic Carbene Ligands in Ru(Ph2PCH2CH2CH2PPh2)(IMes)(CO)H2 and Ru(Ph2AsCH2CH2PPh2)(IMes)(CO)H2 (IMes=1,3-Dimesityl-1,3-Dihydro-2H-Imidazol-2-Ylidene). *Adv. Synth. Catal.* **2003**, *345*, 1111−1114.
(43) Gawin, R.; Tracz, A.; Chwalba, M.; Kozakiewicz, A.; Trzaskowski, B.; Skowerski, K. Cyclic Alkyl Amino Ruthenium Complexes—Efficient Catalysts for Macrocyclization and Acrylonitrile Cross Metathesis. *ACS Catal.* **2017**, *7*, 5443−5449.
(44) Frisch, M. J.; Trucks, W.; Schlegel, H. B.; Scuseria, G. E.; Robb, M. A.; Cheeseman, J. R.; Scalmani, G.; Barone, V.; Mennucci, B.; Petersson, G. A.; et al. *Gaussian 09*, Revision E. 01; Gaussian, 2009; Vol. *11*.
(45) Lu, T.; Chen, F. Multiwfn: A Multifunctional Wavefunction Analyzer. *J. Comput. Chem.* **2012**, *33*, 580−592.
(46) Neese, F. The ORCA Program System. *Wiley Interdiscip. Rev.: Comput. Mol. Sci.* **2012**, *2*, 73−78.
(47) Weigend, F. Accurate Coulomb-Fitting Basis Sets for H to Rn. *Phys. Chem. Chem. Phys.* **2006**, *8*, 1057−1065.
(48) Parrish, R. M.; Burns, L. A.; Smith, D. G. A.; Simmonett, A. C.; DePrince, A. E.; Hohenstein, E. G.; Bozkaya, U.; Sokolov, A. Y.; Di Remigio, R.; Richard, R. M.; et al. Psi4 1.1: An Open-Source Electronic Structure Program Emphasizing Automation, Advanced Libraries, and Interoperability. *J. Chem. Theory Comput.* **2017**, *13*, 3185−3197.
(49) Grimme, S. Supramolecular Binding Thermodynamics by Dispersion-Corrected Density Functional Theory. *Chem.—Eur. J.* **2012**, *18*, 9955−9964.
(50) Ribeiro, R. F.; Marenich, A. V.; Cramer, C. J.; Truhlar, D. G. Use of Solution-Phase Vibrational Frequencies in Continuum Models for the Free Energy of Solvation. *J. Phys. Chem. B* **2011**, *115*, 14556−14562.
(51) Lab, P.; Rodríguez-Guerra, J.; Chen, J.; *Ifunes. Bobbypaton/GoodVibes: GoodVibes v3.0.0.*, 2019.
(52) Sanford, M. S.; Love, J. A.; Grubbs, R. H. Mechanism and Activity of Ruthenium Olefin Metathesis Catalysts. *J. Am. Chem. Soc.* **2001**, *123*, 6543−6554.
(53) Hejl, A. *Controlling Olefin Metathesis through Catalyst and Monomer Design*; California Institute of Technology, 2007.
(54) Śliwa, P.; Kurleto, K.; Handzlik, J.; Rogalski, S.; Żak, P.; Wyrzykiewicz, B.; Pietraszuk, C. Regioselectivity of Stoichiometric Metathesis of Vinylsilanes with Second-Generation Grubbs Catalyst: A Combined DFT and Experimental Study. *Organometallics* **2016**, *35*, 621−628.
(55) Straub, B. F. Origin of the High Activity of Second-Generation Grubbs Catalysts. *Angew. Chem. Int. Ed.* **2005**, *44*, 5974−5978.
(56) Otero-de-la-Roza, A.; Johnson, E. R.; Contreras-García, J. Revealing Non-Covalent Interactions in Solids: NCI Plots Revisited. *Phys. Chem. Chem. Phys.* **2012**, *14*, 12165−12172.
(57) Bader, R. F. W. Atoms in Molecules. *Acc. Chem. Res.* **1985**, *18*, 9−15.
(58) Bader, R. F. W. Quantum Theory of Molecular Structure and Its Applications. *Chem. Rev.* **1991**, *91*, 893−928.
(59) Bader, R. F. W. A Bond Path: A Universal Indicator of Bonded Interactions. *J. Phys. Chem. A* **1998**, *102*, 7314−7323.
(60) Bader, R. F. W.; Matta, C. F. Atomic Charges Are Measurable Quantum Expectation Values: A Rebuttal of Criticisms of QTAIM Charges. *J. Phys. Chem. A* **2004**, *108*, 8385−8394.
(61) Meyer, E. A.; Castellano, R. K.; Diederich, F. Interactions with Aromatic Rings in Chemical and Biological Recognition. *Angew. Chem. Int. Ed.* **2003**, *42*, 1210−1250.
(62) Parrish, R. M.; Parker, T. M.; Sherrill, C. D. Chemical Assignment of Symmetry-Adapted Perturbation Theory Interaction Energy Components: The Functional-Group SAPT Partition. *J. Chem. Theory Comput.* **2014**, *10*, 4417−4431.
(63) Bloom, J. W. G.; Wheeler, S. E. Taking the Aromaticity out of Aromatic Interactions. *Angew. Chem. Int. Ed.* **2011**, *50*, 7847−7849.
(64) Neel, A. J.; Hilton, M. J.; Sigman, M. S.; Toste, F. D. Exploiting Non-Covalent π Interactions for Catalyst Design. *Nature* **2017**, *543*, 637−646.

https://dx.doi.org/10.1021/acs.jpca.0c01354
J. Phys. Chem. A 2020, 124, 3609−3617